Sonochemical synthesis and characterization of magnetic separable Fe$_3$O$_4$-TiO$_2$ nanocomposites and their catalytic properties

Wanquan Jiang[a]; Xueping Zhang[a]; Xinglong Gong[b]; Fangfang Yan[b]; Zhong Zhang[c]

[a] Department of Chemistry, University of Science and Technology of China (USTC), Hefei, PR China [b] CAS Key Laboratory of Mechanical Behavior and Design of Materials, Department of Modern Mechanics, USTC, Hefei, PR China [c] National Center for Nanoscience and Technology, Beijing, PR China

PLEASE SCROLL DOWN FOR ARTICLE

Taylor & Francis
Taylor & Francis Group

Sonochemical synthesis and characterization of magnetic separable Fe$_3$O$_4$–TiO$_2$ nanocomposites and their catalytic properties

Wanquan Jiang[a]*, Xueping Zhang[a], Xinglong Gong[b],
Fangfang Yan[b] and Zhong Zhang[c]

[a]*Department of Chemistry, University of Science and Technology of China (USTC), Hefei 230026, PR China;* [b]*CAS Key Laboratory of Mechanical Behavior and Design of Materials, Department of Modern Mechanics, USTC, Hefei 230027, PR China;* [c]*National Center for Nanoscience and Technology, Beijing 100080, PR China*

A novel sonochemical method is described for the preparation of Fe$_3$O$_4$–TiO$_2$ photocatalysts in which nanocrystalline titanium dioxide particles are directly coated onto a magnetic core. The Fe$_3$O$_4$ nanoparticles were partially embedded in TiO$_2$ agglomerates. TiO$_2$ nanocrystallites were obtained by hydrolysis and condensation of titanium tetraisopropyl in the presence of ethanol and water under high-intensity ultrasound irradiation. This method is attractive since it eliminated the high-temperature heat treatment required in the conventional sol–gel method, which is important in transforming amorphous titanium dioxide into a photoactive crystalline phase. In comparison to other methods, the developed method is simple, mild, green and efficient. The magnetization hysteresis loop for Fe$_3$O$_4$–TiO$_2$ nanocomposites indicates that the hybrid catalyst shows superparamagnetic characteristics at room temperature. Photocatalytic activity studies confirmed that the as-prepared nanocomposites have high photocatalytic ability toward the photodegradation of RhB solution. Furthermore, the photodecomposition rate decreases only slightly after six cycles of the photocatalysis experiment. Thus, these Fe$_3$O$_4$–TiO$_2$ nanocomposites can be served as an effective and conveniently recyclable photocatalyst.

Keywords: sonochemical synthesis; recyclable photocatalyst; TiO$_2$ nanocomposite; rhodamine B degradation

1. Introduction

Over the past two decades, oxide semiconductor mediated photocatalysts have attracted a great deal of attention in the purification of environmental contaminants [1–6]. Among the various oxide semiconductor photocatalysts, TiO$_2$ has proven to be the most suitable material for its long-term chemical stability, powerful oxidation strength, non-toxicity and low cost.

Generally, a photocatalytic reaction is conducted in a solid–liquid suspension system of submicron semiconductor materials, and therefore it requires an additional separation step to remove the catalyst from the treated water. Removing such ultrafine particles from large

---

*Corresponding author. Email: jiangwq@ustc.edu.cn

volumes of water is a difficult process and involves further expense. This presents a major drawback to the application of the hybrid catalyst for treating wastewaters. To overcome the problem of catalyst recovery, a magnetic photocatalyst, comprising a magnetic core coated with photoactive titanium oxide layer, has been developed [7–19]. The fabrication of the magnetic photocatalyst is based on the magnetic separation technique, providing a solution to the solid–liquid separation problem of the photocatalyst particles from the suspended photoreactors. The magnetic core is used to enhance separation properties of the photocatalyst from the treated water, whereas the outer titanium oxide coating is useful for the degradation of organic contaminants.

Many methods have already been established for the preparation of titanium dioxide, the sol–gel technique being the most commonly employed. However, the precipitants derived by sol–gel method are amorphous in nature, and further heat treatment is required in order to induce the crystallization of hydrous titanium dioxide. The heat treatment is considered as a key step in determining the final properties of the prepared samples. A number of processes, which have significant implications on the photoactivity and the magnetic properties of the photocatalyst [9,20], occur during the heat treatment. For example, the heat treatment has been found to cause the reduction of specific surface area (due to sintering and crystal growth) and a loss of surface hydroxyl groups. High temperature calcination of the magnetic photocatalyst also led to the interaction of the magnetic core and the outer titanium dioxide coating. The heat treatment also caused the partial oxidation of the magnetic core, and hence a reduction of magnetic properties of the as-prepared photocatalyst.

Thus an alternative particle preparation method for crystalline TiO_2 was sought in which the heat treatment step was not required. As a competitive alternative, the sonochemical method has been extensively used to generate novel materials with improved or unusual properties. The physicochemical effects of ultrasound arise from acoustic cavitation, i.e. the formation, growth, and implosive collapse of bubbles in a liquid. The collapse of bubbles generates localized hot spots with transient temperatures of 5000 K and cooling rates in excess of 10^{10} K/s. These extreme conditions during sonication lead to enhanced medium mixing and in addition the particle size of the solid present in the reaction medium decreases and the reactive surface area increases [21–23]. However, reports on the coating of crystalline material directly onto magnetic core particles via sonochemistry method are very scarce so far.

In this paper, a simple, mild, efficient sonochemical method is presented for the synthesis of highly photoactive Fe_3O_4–TiO_2 nanocomposites. First, Fe_3O_4 nanoparticles were synthesized by a coprecipitation method. Second, crystalline titanium oxide was directly coated onto the magnetic core by an ultrasound irradiation method for a short time at relatively low temperature (90°C). The heat treatment step required in a typical sol–gel method was eliminated. Characterization was accomplished by using various techniques, such as powder X-ray diffraction (XRD), transmission electron microscopy (TEM), X-ray photoelectron spectroscopy, vibrating sample magnetometry (VSM), and UV/visible absorption spectroscopy (UV/vis).

2. Experimental procedure

2.1. *Synthesis of magnetic nanoparticles*

Fe_3O_4 nanoparticles were prepared by the conventional coprecipitation of Fe(II) and Fe(III) chlorides (Fe^{II}/Fe^{III} ratio = 0.5) with $NH_3 \cdot H_2O$. The final product was magnetically separated and washed several times with water and ethanol after the reaction. The microspheres were dried at 50°C under vacuum.

2.2. Synthesis of Fe₃O₄–TiO₂ nanocomposites

The magnetic nanocomposites were synthesized via a simple sonochemical route. Typically, 0.14 g of the as-prepared Fe_3O_4 nanoparticles was dispersed in 25 ml of ethanol and 50 ml of deionized water and was sonicated for 1 h in air at room temperature. Then a mixture of 2 ml of TTIP and 75 ml of ethanol was added into it dropwise. The sonochemical reaction was carried out by pulsed mode, employing a direct immersion titanium horn in the reaction solution. A high-intensity ultrasonic probe (from Xinzhi Co., China, JY92–2D, with a 6 mm diameter titanium horn of 20 kHz working in a pulsed mode with a duty cycle of 7 s) and a flat-bottomed Pyrex glass vessel (total volume of 200 ml) were used for the ultrasound irradiation. The round-bottom flask was kept at 90°C during the reaction. The total reaction time was continued for 4.5 h so as to complete the crystallization of TiO_2. The resulting product was separated after sonication, washed three times with ethanol and once with deionized water, and further dried at 60°C under vacuum.

2.3. Photocatalytic activity measurement of Fe₃O₄–TiO₂ nanocomposites

The photocatalytic activity of the prepared samples was assessed by using the photocatalytic reaction system shown in Figure 1. The total volume of the photocatalytic reactor was about 50 ml. Before UV illumination, 25 mg of Fe_3O_4–TiO_2 nanocomposites was suspended in 55 ml of rhodamine B (RhB) aqueous solution (1×10^{-5} M). The solution was continuously stirred for about 1 h in the dark to ensure the establishment of an adsorption/desorption equilibrium among the RhB, photocatalyst and water. Then the solution was exposed to UV irradiation from a 300 W high-pressure Hg lamp at room temperature. The suspension (5 ml) was collected at regular intervals to measure the RhB degradation from UV/vis absorption spectra.

2.4. Characterization

XRD patterns of the products were obtained with a Japan Rigaku DMax-γA rotation anode X-ray diffractometer equipped with graphite monochromatized Cu K$_\alpha$ radiation ($\lambda = 0.154178$ nm). TEM photographs were taken on a Hitachi Model H-800 transmission
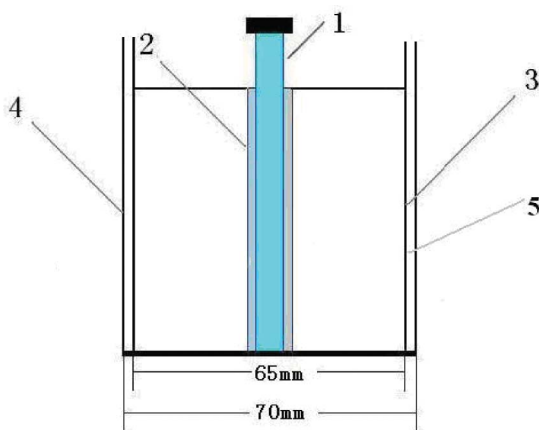

Figure 1.   Photocatalytic reactor: (1) UV lamp; (2) quartz glass cooling sleeve; (3) the inner wall of the reactor; (4) the outer wall of the reactor; (5) the RhB solution.

electron microscope at an accelerating voltage of 200 kV. The high-resolution TEM (HRTEM) images were taken on a JEOL-2010 TEM. X-ray photoelectron spectra (XPS) were measured on an ESCA Laboratory MKII instrument with Mg K_α radiation as the exciting source. The UV/vis spectra were recorded using a UV-365 spectrophotometer.

3.   Result and discussion

3.1.   *Characterization of Fe₃O₄–TiO₂ nanocomposites*

In order to determine the crystal structure and the composition of the as-prepared nanocomposites, an X-ray power diffraction experiment was carried out. Figure 2 shows the XRD patterns of the samples. In Figure 2, the XRD patterns of Fe_3O_4 and Fe_3O_4–TiO_2 nanocomposites present the same set of characterization peaks (30.1°, 35.5°, 43.1°, 53.5°, 56.9°, 62.6°). These peaks come from diffraction of magnetic iron oxide with cubic spinel structure (JCPDS: No. 19-0629). All the diffraction peaks of Fe_3O_4 were maintained after the TiO_2 deposition, which indicated that the effects on crystal structure of the Fe_3O_4 nanoparticles were negligible during the ultrasound irradiation.

The titanium dioxide in the nanocomposites has an anatase structure, as seen from the XRD pattern of Fe_3O_4–TiO_2, where the peaks (25.3°, 37.8°, 48.0°, 53.9°) are the characterization peaks of anatase structure of titanium dioxide (JCPDS: No. 21-1272). The broad nature peak of the deposited TiO_2 is an indication of the small crystallite size. The mean size of a single TiO_2 crystallite can also be determined from the broadening of corresponding X-ray diffraction peaks by using Scherrer's formula:

$$D = \frac{K\lambda}{\beta \cos \theta},\tag{1}$$

where λ is the wavelength of the X-ray radiation ($\lambda = 0.15418$ nm), K is the Scherrer constant ($K = 0.89$), θ is the angle of the X-ray diffraction peak (here $\theta = 12.7°$) and β is the full-width at half-maximum (FWHM) of the (101) plane (here $\beta = 0.68°$) [24]. The estimated crystallite size of TiO_2 was about 12.3 nm.

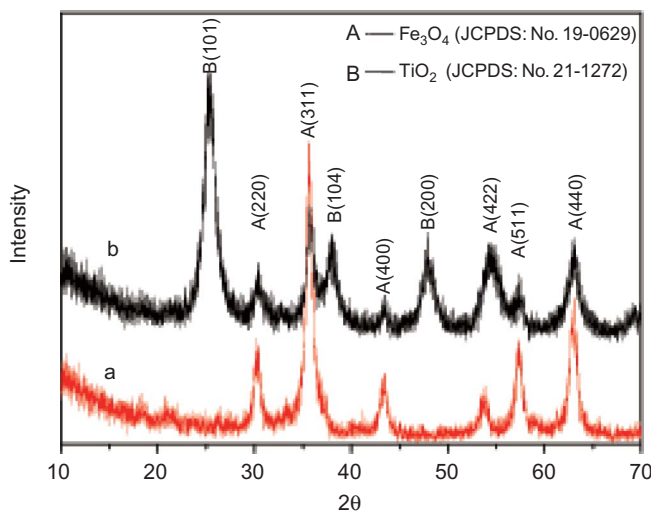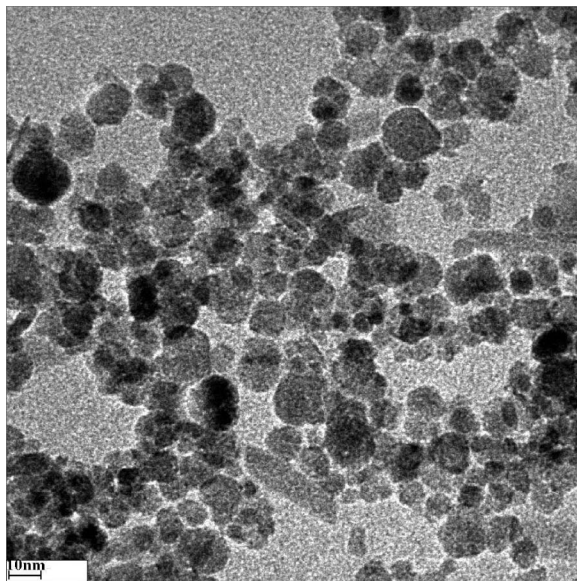Figure 2.   XRD patterns of Fe_3O_4 and Fe_3O_4–TiO_2 nanocomposites.

Figure 3.   TEM images of Fe_3O_4 nanoparticles.

The typical TEM images of Fe_3O_4 shown in Figure 3 revealed that most of the particles were spherical and with an average diameter of 12 nm. Figure 4 shows HRTEM images of the Fe_3O_4–TiO_2 nanocomposites. The crystallite size of TiO_2 is around 12.9 nm in Figure 4a, which is in agreement with the above XRD results, and the shape of particles was mainly spherical. A high-magnification HRTEM was used to further investigate the structure of the Fe_3O_4–TiO_2 sample (Figure 4b). This revealed that the prepared samples were well crystallized, as evidenced by well-defined lattice fringes. The small crystallite size and the well crystallized structure contributed to the efficient photocatalytic property of hybrid catalyst, which was confirmed by the subsequent photocatalytic activity studies of the Fe_3O_4–TiO_2 nanocomposites.

It can be observed that TiO_2 nanocrystal is attached to the Fe_3O_4 nanocrystal, and that the interplanar distance of that nanoparticle is about 0.19 nm, revealing the crystalline nature of the nanocrystal; the interplanar distance of the Fe_3O_4 microspheres is about 0.25 nm and corresponds to its (311) plane. The HRTEM analysis confirmed that both Fe_3O_4 and TiO_2 coexisted in the resulting samples. Furthermore, an interconnected nanoparticle morphology can be observed in Figure 4b, which indicates that a Fe_3O_4–TiO_2 nanocrystal heterojunction is formed in the composite.

XPS analysis was used to elucidate the detailed surface chemical composition of these particles' surface. As shown in Figure 5a, the main peaks are C $1s$, O $1s$ and Fe $2p$ centered at 284.8 eV, 530 eV and 710.5 eV, respectively. In the Fe_3O_4–TiO_2 nanocomposite spectrum (Figure 5b), a new peak appears at 458.8 eV, assigned to the photoelectrons originating from the Ti $2p$ energy level, which responds to the Ti element in the hybrid catalyst. Compared with Fe_3O_4 spectrum, the signal of Fe $2p$ decreases from 16% to 6%, which is in response to the TiO_2 content in Fe_3O_4–TiO_2 nanocomposites. However, there is still considerable residual signal of Fe $2p$ in the spectrum of the Fe_3O_4–TiO_2 nanocomposites. These results suggested that Fe_3O_4 and TiO_2 were present mainly as separated phases in the Fe_3O_4–TiO_2 composites.

(a)

(b)
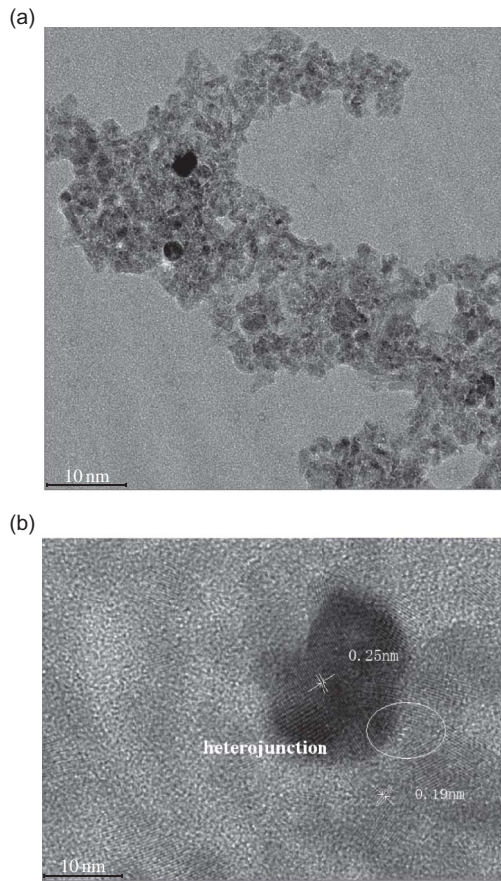
Figure 4. HRTEM images of as-prepared Fe_3O_4–TiO_2 nanocomposites (a, b) with different magnifications.

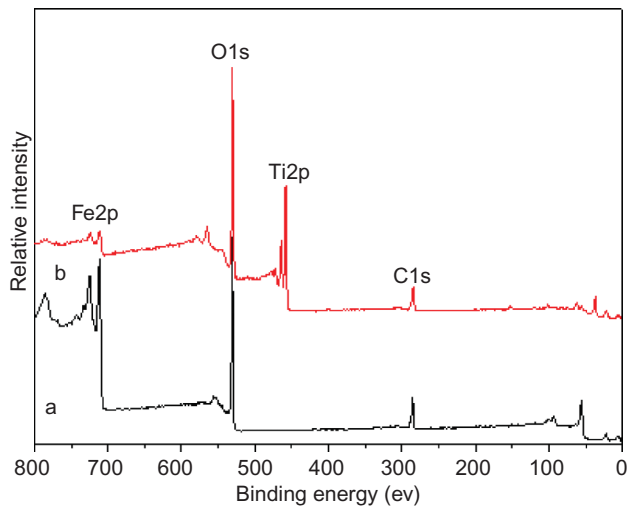Figure 5. XPS of Fe_3O_4 (a) and Fe_3O_4–TiO_2 (b) nanocomposites.

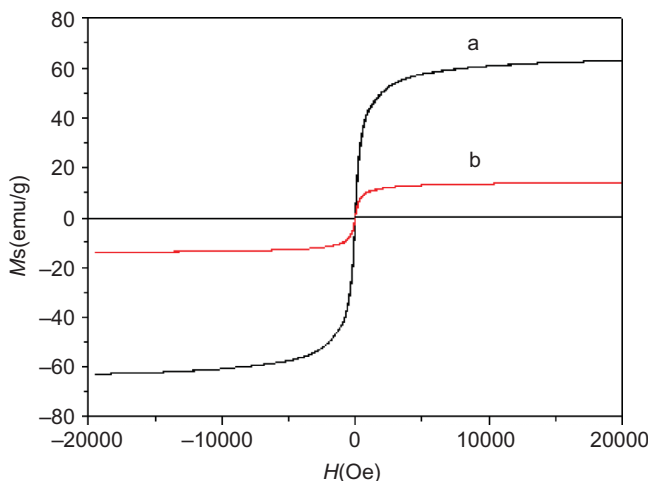Figure 6. *M–H* curves of Fe$_3$O$_4$ (a) and Fe$_3$O$_4$–TiO$_2$ (b) nanocomposites at room temperature.

3.2. *Magnetic properties of Fe$_3$O$_4$/TiO$_2$ nanocomposites*

The magnetic properties of the prepared samples were measured with a VSM. Figure 6 shows the magnetization (*M–H*) curves of the uncoated and coated Fe$_3$O$_4$ nanoparticles. It can be seen that saturation magnetization value of the coated Fe$_3$O$_4$ (14 emu/g) is much lower than that of the bare Fe$_3$O$_4$ (63 emu/g). The decrease in saturation magnetization is mainly due to the non-magnetic titanium dioxide content in the nanocomposites. In addition, the coercivity (*H$_c$*) and remanent magnetization (*M$_r$*) of the Fe$_3$O$_4$–TiO$_2$ nanocomposites are close to zero, indicating that hybrid catalyst exhibits superparamagnetic properties at room temperature. Superparamagnetic properties are very important to the recyclable photocatalytic properties of a hybrid catalyst. With superparamagnetic properties, the magnetic photocatalyst can be recovered efficiently by imparting an external magnetic field and no residual magnetism exists after removal of the applied magnetic field. Therefore, the prepared hybrid catalyst can be easily redispersed in solution for recycling.

3.3. *Sonochemical reaction mechanism*

The hydrolytic species of TTIP in water condensed to form a large number of tiny gel nuclei, which aggregated to form larger clusters. Ultrasound irradiation generates many local hot spots within the gel, outside which the polycondensation of ≡Ti–OH or ≡Ti–OR is promoted [25]. The local hot spot is beneficial to the rapid loss of organic residue and water. This further causes the formation of a large number of seed nuclei, which leads to a smaller grain size. In this case, the preferred region for TiO$_2$ crystallization is the interfacial zone of the ultrasound cavity. This is due to the low vapor pressure of the reactants [26]. Compared with the traditional stirring technology, the sonochemistry has proven to stimulate the speed of the reaction in liquid. Control experiments demonstrated that TiO$_2$ was amorphous in the absence of sonication. Thus, high-intensity ultrasound can accelerate the crystallization of TiO$_2$. In the present work, nanocrystalline products were obtained without calcination.

3.4. *Photocatalytic activity studies of the Fe$_3$O$_4$–TiO$_2$ nanocomposites*

To evaluate the photocatalytic ability of the Fe$_3$O$_4$–TiO$_2$ nanocomposites, RhB dye solution was selected as the model. Typically, 25 mg of the as-prepared samples were added to

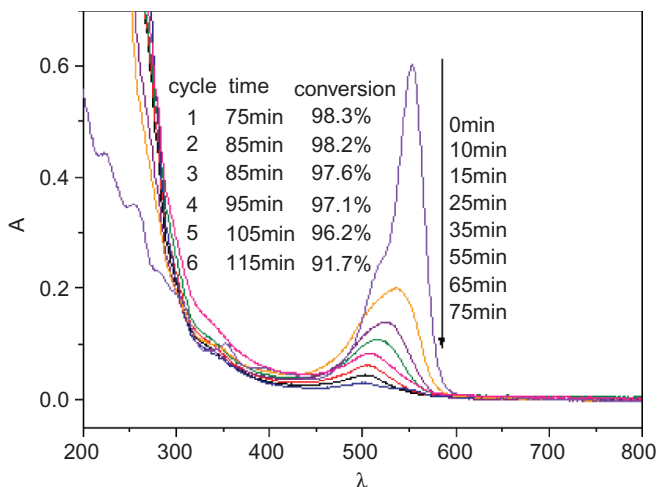Figure 7. UV/vis absorption spectral changes of RhB aqueous solution in the presence of Fe_3O_4–TiO_2 nanocomposites.

55 ml of the 6×10^{-5} M RhB solution, which was then irradiated using a high-pressure Hg lamp. The temporal UV/vis spectra changes of the RhB solution extracted at different time intervals during the photocatalytic degradation reaction are shown in Figure 7. As can be observed from Figure 7, the main absorbance of RhB maximized at ca. 554 nm markedly decreased with irradiation time, and almost completely disappeared after 75 min irradiation. Comparison experiments indicated that decomposition of RhB solution (without any photocatalyst) was very slow and RhB was not degraded by Fe_3O_4–TiO_2 nanocomposite suspensions in the dark. This demonstrates that the photodegradation of RhB in the present study is indeed through a photocatalytic process. Furthermore, it was observed that the main absorbance peak of RhB (at 554 nm) gradually shifted to shorter wavelength and reached 498 nm after 45 min of irradiation; after which the absorbance peak position did not change, whereas the main absorption peak intensity further decreased to 0 after 75 min of irradiation. The hypsochromic shift in λ_{max} of RhB over Fe_3O_4–TiO_2 photocatalysts may be due to the step-by-step de-ethylation of RhB. The absorbance peak centered at 498 nm was assigned to the absorbance of the completely de-ethylated product of RhB, namely rhodamine. The compounds that give absorption peaks position between 498 nm and 554 nm might consist of several partially de-ethylated intermediates, including N,N,N'-triethylated rhodamine (λ_{max} at 539 nm), N,N'-diethylated rhodamine (λ_{max} at 522 nm), and N-ethylated rhodamine (λ_{max} at 510 nm). The blue gradual shift in λ_{max} indicates that the de-ethylation reactions proceeded in stepwise manner. The reduction in the absorbance after the completion of N-de-ethylation was due to the subsequent degradation reaction [27]. This hybrid catalyst presented efficient photocatalytic activity in the degradation of RhB. The photocatalytic activity of TiO_2 depends strongly on crystal structure, particle size and surface area. Titanium dioxide, in its anatase phase, is considered to be one of the most suitable photocatalytic materials [28]. Due to the quantum size effect, when the size of TiO_2 is decreased to nanoscale, the catalytic activity is enhanced and the surface area increased [1]. In our study, the high performance of Fe_3O_4–TiO_2 hybrid catalyst may be attributed to the pure anatase structure and the small particle size of titanium dioxide. In this reaction system, the real photocatalytic

mechanism of the nanocomposites is still unclear, and further relevant work needs to be carried out.

The magnetic property of the nanocomposites is of great use for the efficient recovery and recycling of magnetic photocatalyst in the liquid–solid reaction system. With the superparamagnetic property of the as-prepared samples, upon applying an external magnetic field, the hybrid catalyst can be recovered within 1 min and the solution becomes transparent. The recovery percentage of the used hybrid catalyst was over 98%. As practical recyclable catalysts, high photocatalytic activity of the as-prepared nanocomposites is necessary. To investigate the reusability of the photocatalyst, the as-prepared nanocomposites were subjected to repeated cycles of RhB degradation. First, the catalysts solution was continuously stirred for about 1 h in the dark. Second, the catalysts were magnetically separated after the each run of irradiation, then repeated the first step. In Figure 7, it can be seen that the activity of catalyst decreases slightly after six cycles of photocatalysis experiments. However, the photodecomposition rate of RhB in the last cycle still reached up to 91.7%. In conclusion, sonochemical synthesis of a photocatalyst resulted in good photocatalytic ability. The decrease in the photoactivity of the prepared nanocomposites after each cycle of usage may partly result from the incomplete magnetic separation of hybrid catalyst and the loss of catalyst during the reaction.

4.   Conclusion

A novel sonochemical method for the synthesis of heterogeneous Fe_3O_4–TiO_2 photocatalyst has been reported. Additional heat treatment in conventional sol–gel technique to improve the crystallinity of the prepared samples was eliminated. This method is simple, mild, green, and efficient compared with other routes for the preparation of similar nanostructures. The products exhibit excellent magnetic properties at room temperature, and have high photocatalytic activity toward the degradation of RhB solution; 6×10^{-5} M RhB solution can be decomposed completely within 75 min. The renewable photocatalytic ability decreases slightly after six cycles of usage; however, 91.7% RhB is decomposed in the sixth cycle, which means that the as-prepared hybrid catalyst can be used as an efficient and conveniently recoverable photocatalyst.

Acknowledgements

References

[1] M.R. Hoffmann, S.T. Martin, W.Y. Choi, and D.W. Bahnemann, *Environmental applications of semiconductor photocatalysis*, Chem. Rev. 95 (1995), pp. 69–96.

[2] A. Fujishima, T.N. Rao, and D.A. Tryk, *Titanium dioxide photocatalysis*, J. Photochem. Photobiol. C Photochem. Rev. 1 (2000), pp. 1–21.

[3] A.L. Linsebigler, G. Lu, and J.T. Yates Jr., *Photocatalysis on TiO₂ surfaces: Principles, mechanisms, and selected results*, Chem. Rev. 95 (1995), pp. 735–758.

[4] M.A. Fox and M.T. Dulay, *Heterogeneous photocatalysis*, Chem. Rev. 93 (1993), pp. 341–357.

[5] C.C. Wong and W. Chu, *The hydrogen peroxide-assisted photocatalytic degradation of alachlor in TiO₂ suspensions*, Environ. Sci. Tech. 37 (2003), pp. 2310–2316.

[6] W. Ho, J. Yu, J. Lin, and P. Li, *Preparation and photocatalytic behavior of MoS₂ and WS₂ nanocluster sensitized TiO₂*, Langmuir 20 (2004), pp. 5865–5869.

[7] D. Beydoun and R. Amal, *Implications of heat treatment on the properties of a magnetic iron oxide–titanium dioxide photocatalyst*, Mater. Sci. Eng. B 94 (2002), pp. 71–81.

[8] J.Y. Chen and T.Z. Peng, *Preparation and properties of a magnetic-nanometer TiO$_2$/Fe$_3$O$_4$ composite photocatalyst*, Acta Chim. Sinica 62 (2004), pp. 2093–2097.

[9] D. Beydoun, R. Amal, G. Low, and S. McEvoy, *Novel photocatalyst: Titania-coated magnetite. Activity and photodissolution*, J. Phys. Chem. B 104 (2000), pp. 4387–4396.

[10] F. Chen and J. Zhao, *Preparation and photocatalytic properties of a novel kind of loaded photocatalyst of TiO$_2$/SiO$_2$/γ-Fe$_2$O$_3$*, Catal. Lett. 58 (1999), pp. 245–247.

[11] Y. Gao, B.H. Chen, H.L. Li, and Y.X. Ma, *Preparation and characterization of a magnetically separated photocatalyst and its catalytic properties*, Mater. Chem. Phys. 80 (2003), pp. 348–355.

[12] H.B. Yang, W.Y. Fu, M.H. Li, M.H. Li, N. Yang, and G.T. Zou, *Anatase TiO$_2$ nanolayer coating on cobalt ferrite nanoparticles for magnetic photocatalyst*, Mater. Lett. 59 (2005), pp. 3530–3534.

[13] Y.S. Chung, S.B. Park, and D. Kang, *Magnetically separable titania-coated nickel ferrite photocatalyst*, Mater. Chem. Phys. 86 (2004), pp. 375–381.

[14] R.D.K. Misra, S. Rana, and J. Rawat, *Anti-microbial active composite nanoparticles with magnetic core and photocatalytic shell: TiO$_2$-NiFe$_2$O$_4$ biomaterial system*, Acta Biomater. 1 (2005), pp. 691–703.

[15] F. Chen, Y.D. Xie, J.C. Zhao, and G.X. Lu, *Photocatalytic degradation of dyes on a magnetically separated photocatalyst under visible and UV irradiation*, Chemosphere 44 (2001), pp. 1159–1168.

[16] S. Rana, R.S. Srivastava, M.M. Sorensson, and R.D.K. Misra, *Synthesis and characterization of nanoparticles with magnetic core and photocatalytic shell: Anatase TiO$_2$–NiFe$_2$O$_4$ system*, Mater. Sci. Eng. B 119 (2005), pp. 144–151.

[17] H.B. Yang, W.Y. Fu, L.X. Chang, H. Bala, M.H. Li, and G.T. Zou, *Anatase TiO$_2$ nanolayer coating on strontium ferrite nanoparticles for magnetic photocatalyst*, Colloid Surf. A Physicochem. Eng. Asp. 289 (2006), pp. 47–52.

[18] H.B. Yang, W.Y. Fu, M.H. Li, L.X. Chang, Q.J. Yu, J. Xu, and G.T. Zou, *Preparation and photocatalytic characteristics of core-shell structure TiO$_2$/BaFe$_{12}$O$_{19}$ nanoparticles*, Mater. Lett. 60 (2006), pp. 2723–2727.

[19] H.S. Li, Y.P. Zhang, S.Y. Wang, Q. Wu, and C.H. Liu, *Study on nanomagnets supported TiO$_2$ photocatalysts prepared by a sol–gel process in reverse microemulsion combining with solvent-thermal technique*, J. Hazard. Mater. 169 (2009), pp. 1045–1053.

[20] D. Beydoun, R. Amal, G. Low, and S. McEvoy, *Role of nanoparticles in photocatalysis*, J. Nanopart. Res. 1 (1999), pp. 439–458.

[21] T.J. Mason, *Sonochemistry: The Uses of Ultrasound in Chemistry*, The Royal Society of Chemistry, Cambridge, 1990.

[22] G.J. Price, *Current Trends in Sonochemistry*, The Royal Society of Chemistry, Cambridge, 1992.

[23] J.C. Yu, J. Yu, W. Ho, and L. Zhang, *Preparation of highly photocatalytic active nano-sized TiO$_2$ particles via ultrasonic irradiation*, Chem. Comm. (2001), pp. 1942–1943.

[24] Y.B. Xie and C.W. Yuan, *Visible-light responsive cerium ion modified titania sol and nanocrystallites for X-3B dyedegradation*, Appl. Catal. B Environ. 46 (2003), pp. 251–259.

[25] W. Huang, X. Tang, Y. Wang, Y. Koltypin, and A. Gedanken, *Selective synthesis of anatase and rutile via ultrasound irradiation*, Chem. Comm. (2000), pp. 1415–1416.

[26] P. Jeevanandam, Y. Koltypin, Y. Mastai, and A. Gedanken, *Sonochemical synthesis of lead hydroxy bromide needles*, J. Mater. Chem. 10 (2000), pp. 2143–2146.

[27] X.K. Li and J.H. Ye, *Photocatalytic degradation of rhodamine B over Pb$_3$Nb$_4$O$_{13}$/fumed SiO$_2$ composite under visible light irradiation*, J. Phys. Chem. C 111 (2007), pp. 13109–13116.

[28] W.Y. Fu, H.B. Yang, M.H. Li, M.H. Li, N. Yang, and G.T. Zou, *Anatase TiO$_2$ nanolayer coating on cobalt ferrite nanoparticles for magnetic photocatalyst*, Mater. Lett. 59 (2005), pp. 3530–3534.